THE EFFECT OF DIDYMOS INTERNAL STRUCTURE ON PARTICLE DYNAMICS NEAR ITS SURFACE

S. Soldini[1], F. Ferrari[2], Y. Zhang[3], S. Raducan[4], M. Jutzi[4], M. P. Molina[5], A. C. Bagatin[5], D. C. Richardson[3], K. Tsiganis[6], O. Karatekin[7], O. S. Barnouin[8], T. Daly[8], C. M. Ernst[8], E. Palmer[9], A. S. Rivkin[8], N. L. Chabot[8] and the DART Investigation Team, [1]University of Liverpool, Liverpool, UK; stefania.soldini@liverpool.ac.uk; [2]Politecnico di Milano, Milan, Italy; [3]University of Maryland, College Park, MD, USA; [4]University of Bern, Bern, Switzerland; [5]Universidad da Alicante, Alicante, Spain; [6]Aristotle University of Thessaloniki, Thessaloniki, Greece; [7]Royal Observatory of Belgium, Brussels, Belgium; [8]Johns Hopkins University Applied Physics Laboratory, Maryland, USA; [9]Planetary Science Institute, Tucson, USA

Keywords: *Didymos, Rubble-Pile Asteroids, Mascons Gravity Model, Polyhedron Gravity Model, DART mission*

Introduction: On 26th September, 2022, the DART spacecraft intentionally impacted on Dimorphos, the secondary member of the Didymos system, successfully demonstrating the first planetary defense test in space [1]. The images captured by the DRACO camera [1] and LICIACube [2] have provided an initial understanding of the local topography of both Didymos and Dimorphos. Thus, a preliminary estimation of both asteroids' shapes models is now available [1]. In this work, we examine the internal rubble-pile structure of Didymos by using the numerical model PKDGRAV to estimate dynamical properties due to variations in internal structure and grain density. To cross-compare different internal structure models, a sphere-cluster-based gravity model (mascons) is used. This method provides a semi-analytical expression of the linearised equations around the asteroids' gravitational equilibrium [3] and an easy way to search for families of periodic orbits around them.

The mascons gravity model can retrieve the same dynamical properties (e.g., equilibrium points) as a polyhedron gravity model when a uniform bulk density is assumed, only faster. The dynamics are solved for a rotating asteroid-fixed frame with angular velocity equivalent to the asteroid spin. The mascons gravity model has the advantage of providing the same particle mesh distribution for both impact models and astrodynamics, providing an opportunity for a direct link of the two. In this work, the generalised methodology derived by Soldini et al. [4] for asteroid Ryugu [3] is used to study the dynamics around Equilibrium Points (EPs) of Didymos [5].

At the core of our study, a comparison among different initial conditions for the rubble-pile models is performed by evaluating dynamical properties and global gravity information as Stokes coefficients. The evaluation of the dynamical properties of Didymos constrains the assumption made for the internal structure and provides a direct comparison of models. Moreover, this study provides a database of expected gravity estimates that is beneficial for the inverse problem of estimation of the asteroid internal properties from Hera's gravity measurements during the Juventas CubeSat radio science campaign [6].

Mascons Gravity Model:

In this article, the gravity of an irregular-shape body is modeled with a cluster of spheres ("mascons"). Each spherical particle contributes to the overall gravity field of the body. The exterior gravity potential of each sphere behaves as a single point mass. The potential of the irregular body is the sum of each point mass's potential and contributes to the overall potential field:

$$U_{sph} = \sum_{i=1}^{N_{sph}} \left(\frac{G m_i}{|r - r_i|} \right), \tag{1}$$

where m_i ($i = 1, \ldots, N_{sph}$) is the mass of each mascon for a total of N_{sph} masses. r is the distance from the field point to the center of the reference frame (aligned with the center of mass of the asteroid). r_i is the distance of each mass to the reference frame. The total mass of the asteroid is conserved and given by:

$$m_b = \sum_{i=1}^{N_{sph}} m_i. \tag{2}$$

For the mascons gravity model, the gradient of U_{sph} is simply given by:

$$\nabla U_{sph} = -\sum_{i=1}^{N_{sph}} \left(\frac{G m_i}{|r - r_i|^3} \begin{Bmatrix} X - X_i \\ Y - Y_i \\ Z - Z_i \end{Bmatrix} \right), \tag{3}$$

which is the acceleration of the mascons gravity model, i.e., $a_{sph} = \nabla U_{sph}$. The equilibrium equations for the mascons gravity model, for which $\nabla \Omega = 0$, are a nonlinear system of algebraic equations [4], where Ω is the effective potential:

$$\Omega = \frac{1}{2}\omega^2 (X^2 + Y^2) + U_{sph}. \tag{4}$$

where ω is the angular rotation speed of Didymos with spin axis assumed aligned with the z-axis.

The equilibrium positions are thus sensitive to the mascons' resolution (N_{sph}), their coordinates (r_i) and grain density (or masses, m_i). The equilibria are an indicator of how the surface of the asteroid is prone to escape and whether particles can survive in orbit around it. The zero-velocity curves provide a qualitative indication of particles' motion; these are the isolines where velocities are zero for a fixed value in the effective potential, Ω. They represent a qualitative indicator of motions boundaries.

The Stokes coefficients are a measure of the gravity potential and can be derived combining observations of a spacecraft orbit with measurement of the gravity field on board the spacecraft. For a fixed number of masses, N_{sph}, we have:

$$\bar{C}_{n,m} = \frac{1}{m_b(2n+1)} \sum_{i=0}^{N_{sph}} \left(\frac{r_i}{R_b}\right)^n \bar{P}_{n,m}[\sin(\phi_i)] \cos(m\lambda_i) m_i \tag{5}$$

and

$$\bar{S}_{n,m} = \frac{1}{m_b(2n+1)} \sum_{i=0}^{N_{sph}} \left(\frac{r_i}{R_b}\right)^n \bar{P}_{n,m}[\sin(\phi_i)] \sin(m\lambda_i) m_i \tag{6}$$

where $\bar{P}_{n,m}$ is the Legendre Polynomial while $\bar{C}_{n,m}$ and $\bar{S}_{n,m}$ are dimensionless (Stokes) coefficients. Global gravity field solutions are typically provided in the form of a set of Stokes coefficients. The indices n and m in Eq. (5-6) are the degree and order, respectively, of the Legendre function. Having fixed the degree n and order m, the Stokes coefficients represent integrals of functions of the mass distribution of a celestial object. They are a function of the number of masses, N_{sph}, and the position of the mass (m_i) in spherical coordinates (r_i, λ_i, ϕ_i). For zero order, the $\bar{S}_{n,0}$ vanish and the remaining coefficients $\bar{C}_{n,0}$ are refereed to as zonal coefficients. We recall that the second degree zonal Stokes coefficients represent the moments of inertia. The relationship between spherical and Cartesian coordinates is:

$$r_i = \sqrt{x_i^2 + y_i^2 + z_i^2} \tag{7}$$

$$\phi_i = \arcsin \frac{z_i}{r_i} \tag{8}$$

$$\lambda_i = \arctan \frac{y_i}{x_i} \tag{9}$$

When the center of mass is at the reference frame origin, as we have assumed here, the $n = 1$ Stokes coefficients are zero.

Polyhedron and Mascons Gravity Models:

In this section, the normalised gravity coefficients of Didymos as a function of the rubble-pile internal structure is investigated. The aim is to provide a database of expected gravity measurements that ESA's Hera mission could use as a priori assumptions for gravity estimation. Moreover, the mascons gravity model is used for comparing across rubble-pile models. Didymos' mass is assumed to be $5.54687 \cdot 10^{11}$ kg with a spin axis period of 2.26 hours [1]. The bulk density is uncertain and it is now estimated as 2400 $\pm$ 300 kg/m^3 from the DART mission's data [1]. The polyhedron gravity model is here used as a benchmark for determining the resolution (i.e., number) of the mascons gravity model by looking at the 1:1 resonances as shown later in the article. The uniform density distribution case is used for comparing polyhedron and mascons gravity models since the polyhedron model assumes uniform bulk density. The equilibrium points for the polyhedron gravity model were computed with a bulk density of 2700 kg/m^3 as shown in Fig. 1. This bulk density was chosen because is the only case where external equilibrium exists for Didymos.

Figure 1 shows the shape model of Didymos obtained with the DART mission's data [1], the zero velocity curves and the equilibrium points (marked in red in the figure). The Didymos shape model was reduced from the original high resolution model to 3074 vertices and 6144 faces (Fig. 1.a) for computational speed purposes. It was evaluated that 1.2M mascons were an adequate number of masses to retrieve the same dynamical properties (i.e., EPs) of the polyhedron gravity model. Table 1 shows the error in the EPs' positions between the mascons and polyhedron gravity models. The error is within the navigation accuracy of a meter and therefore within of acceptable accuracy [5]. Consequently, the 1.2M mascons number and positions are now kept fixed across all the rubble-piles models and only the grain density of each individual masses is varied for the scope of this analysis. Table 2 shows the positions of the equilibrium points for a bulk density of 2700 kg/m^3 used for this benchmark to determine the number of mascons.

From now a mascons resolution of 1.2M is used, while the grain density was varied, keeping the bulk density within the estimated range of Didymos. The normalised gravity coefficients are computed using the gravity field of the mascons model. The case of homogeneous density distribution is

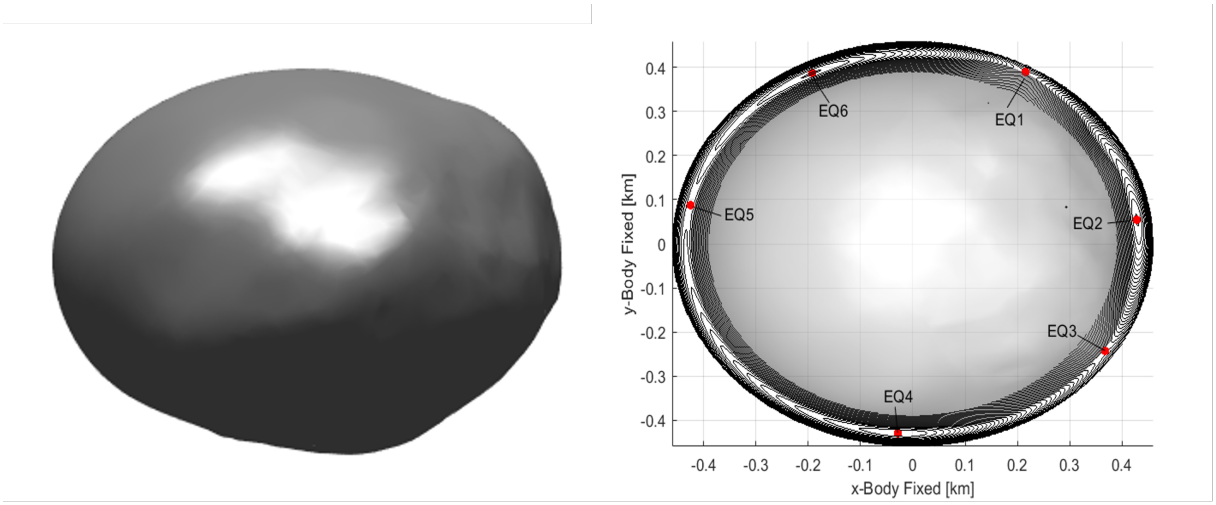

(a) Didymos Shape Model: 3074 vertices and 6144 Faces

(b) Zero velocity curves: polyhedron gravity model (2700 kg/m^3)

Figure 1: Didymos shape model, zero velocity curves and EPs for a homogeneous density distribution.

Table 1: Position error (mascons vs polyhedron) in the equilibrium points for bulk density of 2700 kg/m^3: 1.2M mascons vs 3074 vertices and 6144 faces polyhedron.

EQ	Err X [km]	Err Y [km]	Err Z [km]
1	+8.3181e-05	+5.3739e-04	+4.4024e-04
2	+7.7886e-04	-5.6683e-03	+1.2792e-04
3	+1.5161e-03	+2.2038e-03	-1.0227e-04
4	-2.2670e-02	+1.8837e-03	+1.1131e-03
5	-4.8975e-03	-2.9388e-02	-1.6044e-04
6	+7.7157e-03	+3.7314e-03	-1.3952e-04

Table 2: Equilibrium points for bulk density of 2700 kg/m^3 .

EQ	x [km]	y [km]	z [km]
1	2.1607e-01	3.8892e-01	2.2348e-03
2	4.2853e-01	5.4782e-02	4.4833e-04
3	3.6832e-01	-2.4336e-01	5.1637e-03
4	-2.8334e-02	-4.2983e-01	-3.6362e-03
5	-4.2527e-01	8.8588e-02	2.7166e-04
6	-1.9219e-01	3.8706e-01	-3.2258e-04

assumed and the normalised gravity coefficients for the nominal bulk density of 2400 kg/m^3, its minimum value at 2100 kg/m^3 and its maximum at 2700 kg/m^3 were compared. The normalised gravity coefficients are identical (with error on the order of 10^{-14}) within the range of the analysed bulk densities, as shown in Table 3 normalised gravity coefficients up to order 5. To determine the coefficients in Table 3 that correspond to each bulk density, additional measurements of the acceleration of the gravity field (or gravity effective potential) are needed. Indeed, it can be noticed that EPs are unique to each asteroids and their number and location is determined by the bulk density allowing thus to remove the ambiguity of the normalised gravity coefficients for the homogeneous bulk density case.

Figure 2 shows the gravity effective potential for z-axis coordinates equal to zero (left column Fig.2a,2c,2e) and the correspondent contour lines of the effective potential at a fixed energy level known as zero velocity curves (right column Fig.2b,2d,2f). Each row of figure shows the changes in the effective potential as a function of the bulk density. Note that the maximum and minimum of the potential correspond to an equilibrium condition. The equilibrium points were computed using a set of algebraic equations as shown in [4]. We assumed a spin axis period of Didymos of 2.26 hours and a rotating asteroid-fixed reference frame. As shown in Fig. 2, no equilibrium points can be located externally to the asteroid for bulk densities below and equal 2400 kg/m^3. In this case, the entire surface of Didymos is prone to

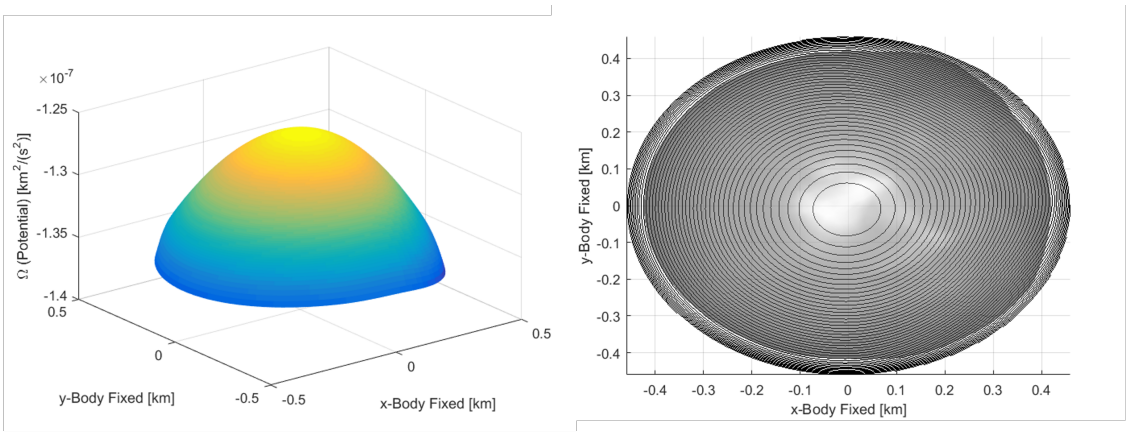

(a) Effective gravity potential (2100 kg/m^3) (b) Zero velocity curves (2100 kg/m^3)

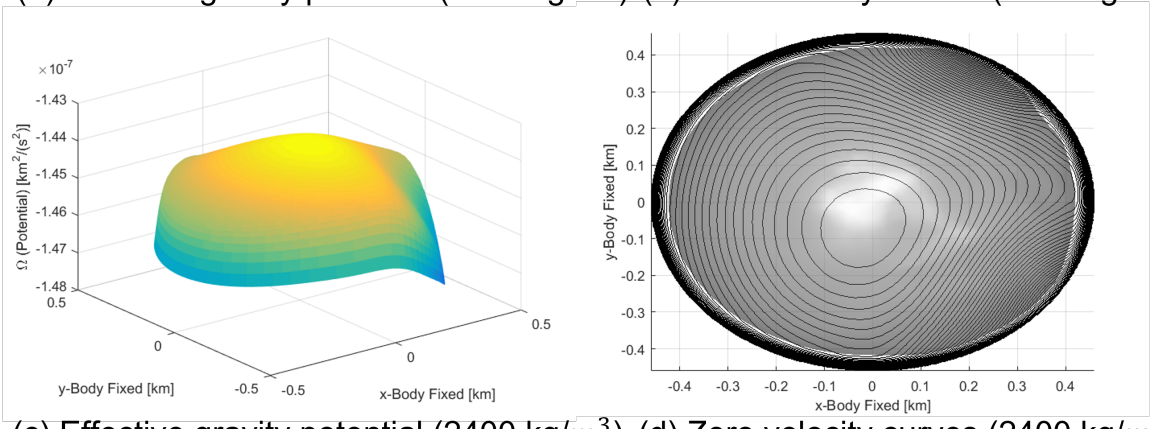

(c) Effective gravity potential (2400 kg/m^3) (d) Zero velocity curves (2400 kg/m^3)

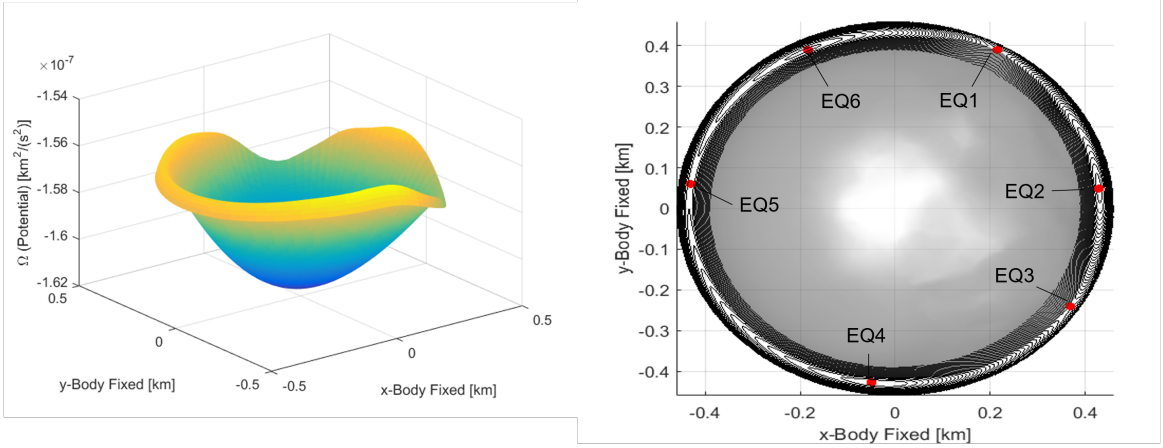

(e) Effective gravity potential (2700 kg/m^3) (f) Zero velocity curves (2700 kg/m^3)

Figure 2: Effective gravity potential and zero velocity curves for a homogeneous density distribution.

escape thus particles could be naturally ejected from its surface. This is due the fast rotational spin period of the asteroid close to its critical value and a low bulk density. On the other hand, a higher bulk density of 2700 kg/m^3 shows the existence of six equilibrium as shown in Table 2 and Fig. 2f. Three equilibrium points are unstable (EQ1,3,5) and three are stable (EQ2,4,6) which imply a

Table 3: Didymos's normalised gravity coefficients with bulk density of 2400 $\pm$ 300 kg/m^3 .

n	m	$\bar{C}_{nm}$	$\bar{S}_{nm}$
1	0	+1.416664754663e-03	+0.000000000000e+00
1	1	+1.881746685161e-03	+1.986554241228e-03
2	0	-4.287084750245e-02	+0.000000000000e+00
2	1	+5.779965851224e-04	+2.007217485344e-03
2	2	+5.056388811032e-04	-2.656306450253e-04
3	0	-1.363253182828e-04	+0.000000000000e+00
3	1	-1.142983508210e-03	+2.097995640852e-04
3	2	-1.035669655004e-04	+1.843635762502e-03
3	3	-1.774092562740e-03	-1.434182137718e-03
4	0	+6.394238605578e-03	+0.000000000000e+00
4	1	-1.507996925742e-04	-6.338701117798e-04
4	2	+2.282847119060e-04	+2.620381767943e-05
4	3	-3.884511757634e-04	+2.749303721090e-04
4	4	-1.208818033100e-03	-1.300490501609e-03
5	0	+2.669070723811e-05	+0.000000000000e+00
5	1	+4.546520617085e-05	+9.492048537159e-05
5	2	-3.043750979216e-04	-6.318946595740e-05
5	3	+6.043103165082e-04	+4.023492310088e-05
5	4	-5.769361785985e-04	-6.946114315462e-04
5	5	-3.542467803933e-04	-5.626719053157e-04

Table 4: Didymos's normalised $\bar{C}_{nm}$ gravity coefficients with bulk density of 2400 kg/m^3 for 64K and 1.2M Masconcs.

n	m	$\bar{C}_{nm}$ (64K)	$\bar{C}_{nm}$ (1.2M)
1	0	-6.082194018631e-18	+2.895472261642e-04
1	1	-1.255233151872e-17	+1.661322558695e-03
2	0	-5.323234360845e-02	-4.370112487191e-02
2	1	+7.885047325186e-04	+6.535879495024e-04
2	2	+5.978994840862e-04	+5.001293210332e-04
3	0	+8.393960737364e-05	+2.224944768938e-06
3	1	-1.171807699891e-03	-1.054626963302e-03
3	2	-2.159806244385e-04	-2.079622571889e-04
3	3	-2.514489591597e-03	-1.824278946312e-03
4	0	+9.569053912375e-03	+6.569235499624e-03
4	1	-3.862381505527e-04	-2.818093479758e-04
4	2	+3.699679457578e-04	+2.407497318070e-04
4	3	-5.811350043890e-04	-4.087607034393e-04
4	4	-2.104043367865e-03	-1.457357817125e-03
5	0	+9.761880579047e-05	+7.780948197416e-05
5	1	+4.032008484328e-05	+6.172035485374e-05
5	2	-3.700046297284e-04	-2.075838756545e-04
5	3	+9.584740102237e-04	+6.215356468256e-04
5	4	-1.186453827448e-03	-7.913434793773e-04
5	5	-5.419683506587e-04	-3.516516262572e-04

more complex motion evolution in the vicinity of Didymos surface. In order to remove the ambiguity posed by the normalised gravity coefficients, it is recommend to estimate the trajectory of particles that might be naturally ejected by Didymos itself similarly to the case of Bennu [7] or to observe DART's impact ejecta particles or boulders orbiting around the system that might have survived once Hera mission arrives to the system. Our previous study performed with bulk density of 2170 $\pm$ 350 kg/m^3 and the shape model estimated before DART mission showed that Didymos displayed one stable equilibrium point (EQ1) for a bulk density of 2170 kg/m^3, while eight equilibrium points were found for a bulk density of 2520 kg/m^3 [8]. It is important to note that the equilibrium points are closely located to Didymos surface and the local topography of the asteroid affects their numbers and positions. Indeed, it is expected that once Hera mission will estimate Didymos' bulk density and local topography the number and location of the equilibrium points can change.

PKDGRAV Rubble-Pile Mascons Gravity Model:

Several PKDGRAV rubble-pile internal structure distributions for the nominal fixed value of bulk density of 2400 kg/m^3, Fig. 3, are here investigated. The PKDGRAV rubble-pile models presented here fit the shape model of Fig. 1.a. Figure 3 shows the PKDGRAV model composed of 46k spheres with the assumption for a homogeneous bulk density. As PKDGRAV uses spheres, we first replaced each sphere with an equivalent mascon for a total of 64K mascons and later the resolution was increased to 1.2M mascons as for the case of the polyhedron. As one can see from the gravity coefficients in Tab. 4-5, the gravity coefficients are affected by the number of Mascons. This is because the original PKDGRAV resolution of 64K is too low for an adequate representation of the Mascons gravity field. Moreover, the gravity coefficients of the PKDGRAV rubble-pile sphere packing model in Tab. 4-5 differs considerably from the homogeneous model of the polyhedron case in Tab. 3. This is due the presence of material voids in the PKDGRAV rubble-pile model in comparison with a solid continuous model as in the polyhedron case or with a uniformly distributed mascons of 1.2M resolution.

Figure 4 shows the effective potential and zero velocity curves for a rubble-pile homogeneous model with bulk density of 2400 kg/m^3 for 64K (Fig.

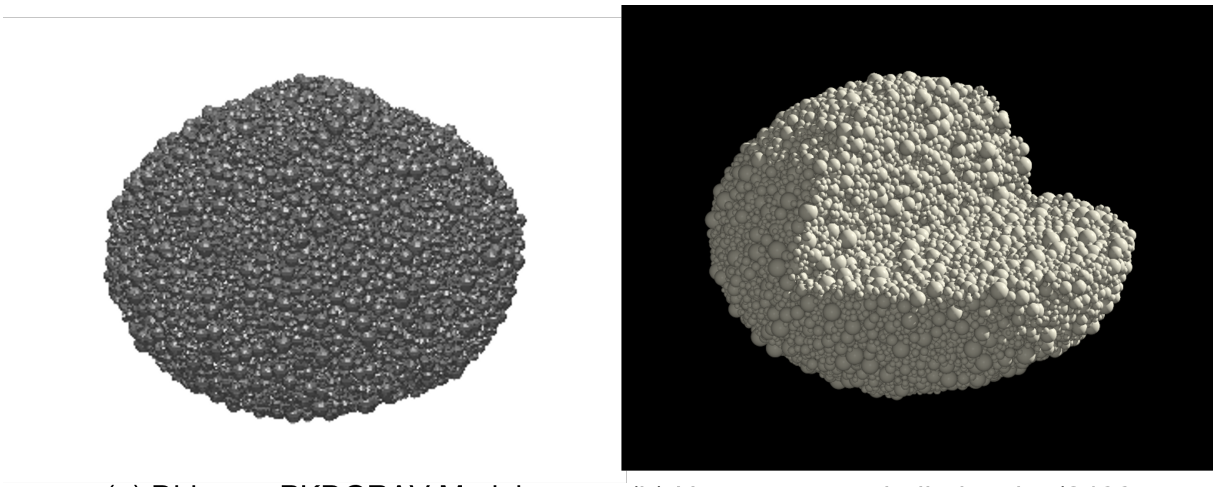

(a) Didymos PKDGRAV Model: 46K spheres

(b) Homogeneous bulk density (2400 kg/m^3)

Figure 3: PKDGRAV Model with 46k spheres and homogeneous bulk density of 2400 kg/m^3 [9, 10].

Table 5: Didymos's normalised $\bar{S}_{nm}$ gravity coefficients with bulk density of 2400 kg/m^3 for 64K and 1.2M Masconcs.

n	m	$\bar{S}_{nm}$ (64K)	$\bar{S}_{nm}$ (1.2M)
1	0	-6.082194018631e-18	+0.000000000000e+00
1	1	-1.255233151872e-17	+9.549164455191e-04
2	0	-5.323234360845e-02	+0.000000000000e+00
2	1	+7.885047325186e-04	+2.142761963630e-03
2	2	+5.978994840862e-04	-2.926345380413e-04
3	0	+8.393960737364e-05	+0.000000000000e+00
3	1	-1.171807699891e-03	+3.735766648663e-04
3	2	-2.159806244385e-04	+2.041776210558e-03
3	3	-2.514489591597e-03	-1.547928680891e-03
4	0	+9.569053912375e-03	+0.000000000000e+00
4	1	-3.862381505527e-04	-6.551107343780e-04
4	2	+3.699679457578e-04	+1.826448966305e-05
4	3	-5.811350043890e-04	+3.964783920031e-04
4	4	-2.104043367865e-03	-1.412140675242e-03
5	0	+9.761880579047e-05	+0.000000000000e+00
5	1	+4.032008484328e-05	+7.800781094902e-05
5	2	-3.700046297284e-04	-1.043265867782e-04
5	3	+9.584740102237e-04	+9.554710251583e-05
5	4	-1.186453827448e-03	-8.765657329660e-04
5	5	-5.419683506587e-04	-5.132517110546e-04

4.a-.b) and 1.2M (Fig. 4.c-.d) masconcs resolution respectively. As one can see, lower mascons resolution in rubble-piles increases the singularity effect from larger voids among mascons as for the case of 64K (Fig. 4.a-.b) mascons while a smoother solution can be found by increasing the resolution to 1.2M (Fig. 4.c-.d). However, it is interesting to compare the case of polyhedron in Fig. 2.c-d. with the PKDGRAV rubble-pile (Fig. 4.c-.d) with same bulk density and mascons resolution. As the rubble-pile sphere packing model presents non uniformly distributed voids, the mascons display small singularities between the voids which is also reflected in the gravity coefficients of Tab. 3 and Tab. 4-5.

Figure 5 shows the assumed PKDGRAV rubble-pile models for Didymos [9, 10] and Table 6-7 show their correspondent normalised gravity coefficients up to order 5. A mascon resolution of 1.2M has been used for the results here presented. The normalised gravity coefficients in Table 6-7 are the a priori value whether the rubble-pile presents an internal structure as shown for Fig. 5. The J_2 term is associated to the $\bar{C}_{20}$ term. If higher order measurements can be estimated by Hera mission beyond the J_2 value it would be possible to discriminate among these solutions. However, as previously demonstrated, uncertainties in the bulk density might not be resolved by measuring solely the normalised gravity coefficients. Figure 5 shows the case of loser core below 200 (Fig. 5.a) and 300 (Fig. 5.b) meters from the center with bulk density of 2325.28 kg/m^3 and 2271.91 kg/m^3 respectively. While, the case of denser core below 200 (Fig. 5.c) and 300 (Fig. 5.d) meters from the center

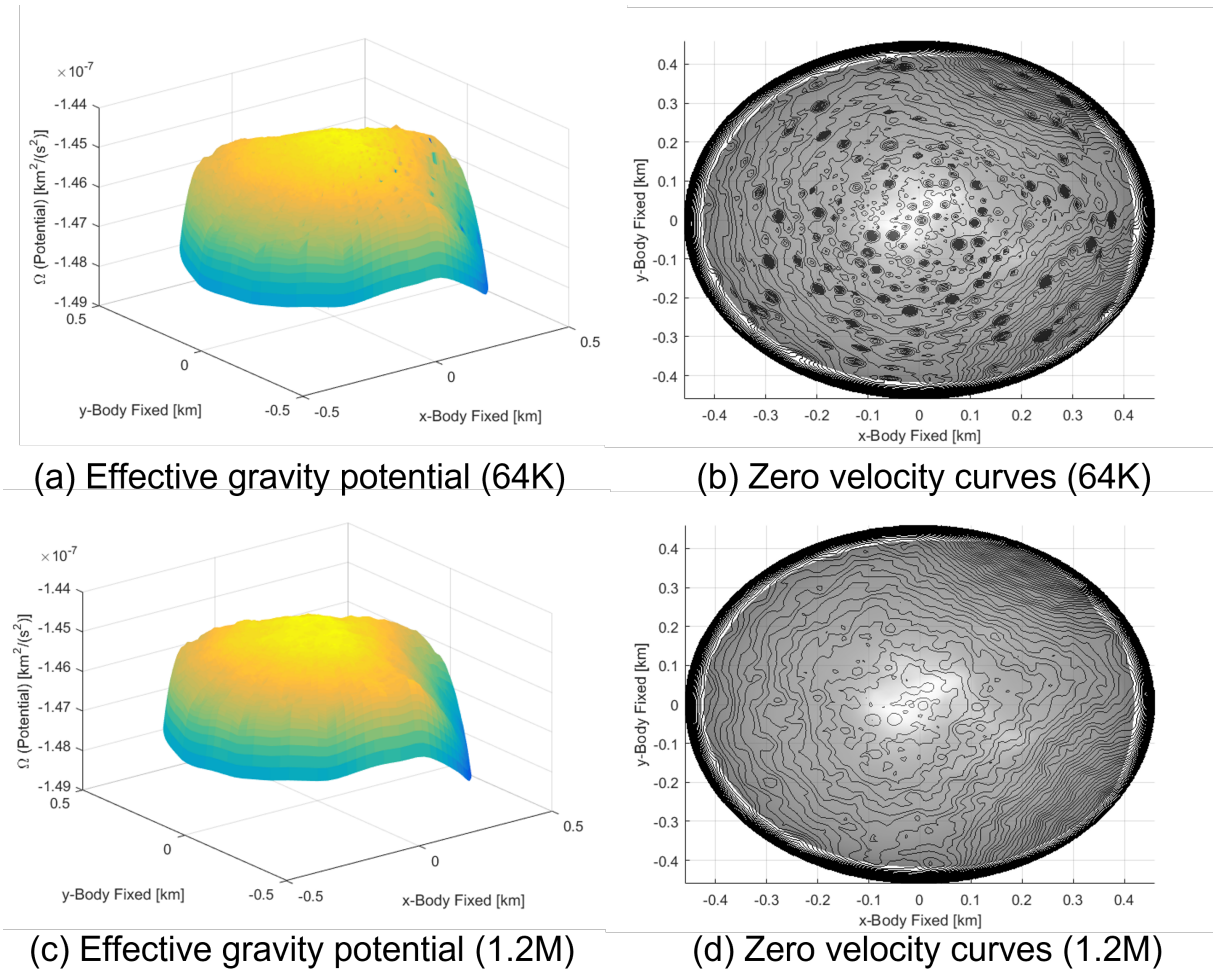

Figure 4: Effective gravity potential and zero velocity curves for a rubble-pile homogeneous model with bulk density of 2400 kg/m^3 for a 64K and 1.2M Mascons resolution.

correspond to bulk density of 2474.26 kg/m^3 and 2516.18 kg/m^3 respectively.

The effective gravity potential and the zero velocity curves for the PKDGRAV rubble-pile models presented in Fig. 5 is now investigated. Figure 6 shows the case of bulk density with looser core. In this case, as for the polyhedron model, a bulk density below 2400 kg/m^3 means that the surface of Didymos is prone to escape as there are no equilibrium points external to the asteroid. Figure 7 shows the case of bulk density with denser core above 2400 kg/m^3. While, there are no equilibrium points outside the shape of Didymos, it is important to notice an interesting pattern in the ridge of the effective potential.a-.c shown in Fig. 7.a-.c. Indeed, the potential ridge presents maximum (yellow) and minimum (marked with a red arrow) regions right below a thin substrate material.

The minimum in the potential corresponds to unstable regions where particle are prone to escape while the maximum represents areas of stability. It is not possible to identify equilibrium points precisely as absolute maximum an minimum can't be identified due to the presence of non uniform voids between particles. However, it is possible to gain an insight on the dynamics stability of rubble-piles.

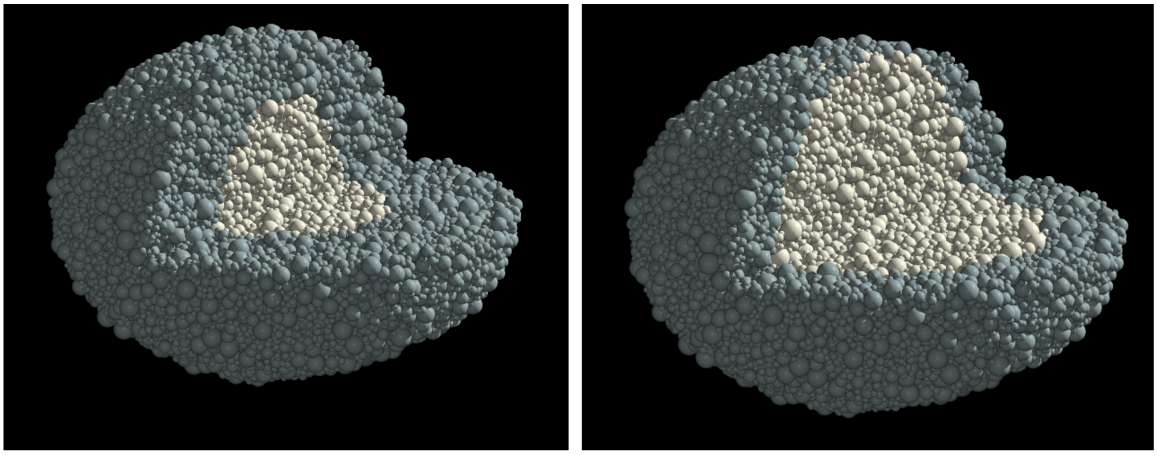

(a) Looser core 200 (2325.28 kg/m^3) (b) Looser core 300 (2271.91 kg/m^3)

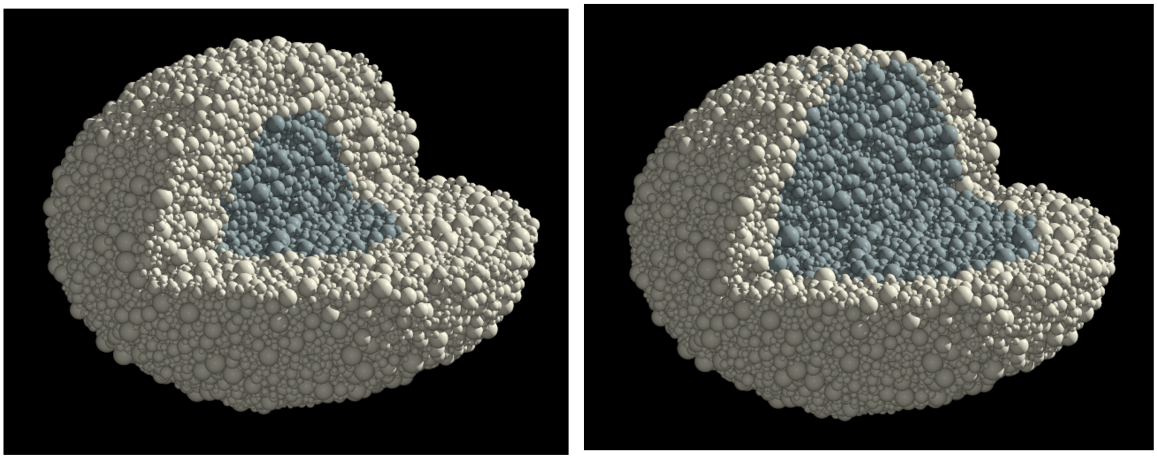

(c) Denser core 200 (2474.26 kg/m^3) (d) Denser core 300 (2516.18 kg/m^3)

Figure 5: Assumed rubble pile internal structure distribution of Didymos with bulk density of 2170 kg/m^3 [9, 10].

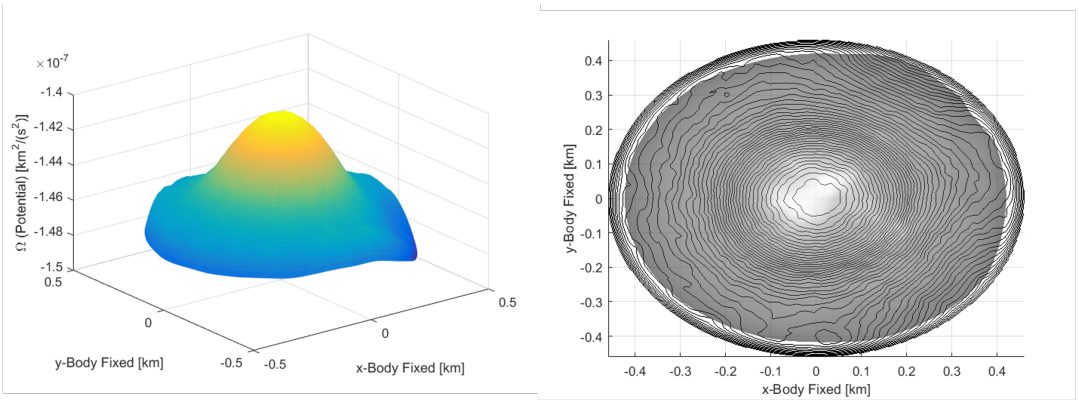

(a) Effective gravity potential (2325.28 kg/m^3) (b) Zero velocity curves (2325.28 kg/m^3)

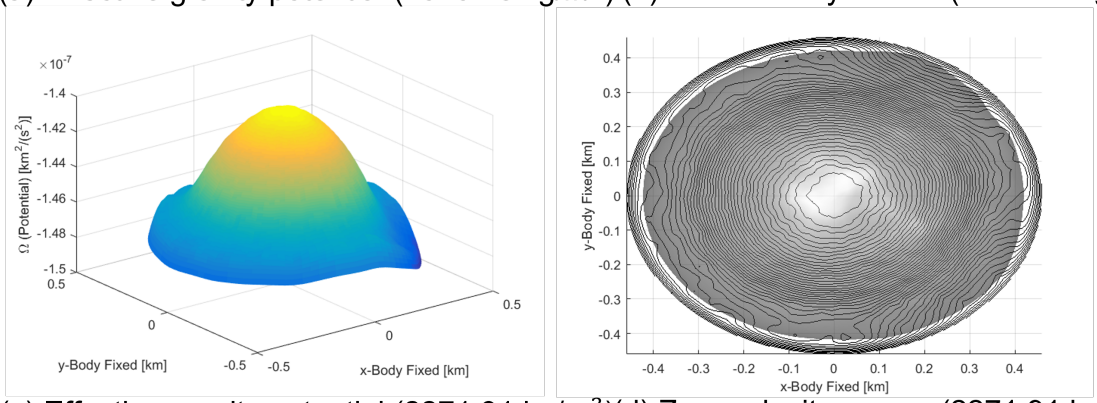

(c) Effective gravity potential (2271.91 kg/m^3) (d) Zero velocity curves (2271.91 kg/m^3)

Figure 6: Effective gravity potential and zero velocity curves for a rubble-pile with looser core as shown in Fig. 5.a-.b.

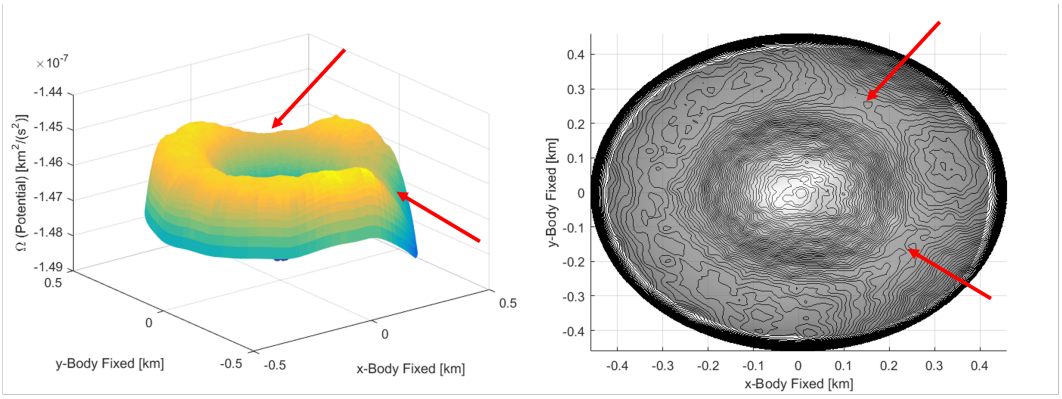

(a) Effective gravity potential (2474.26 kg/m^3) (b) Zero velocity curves (2474.26 kg/m^3)

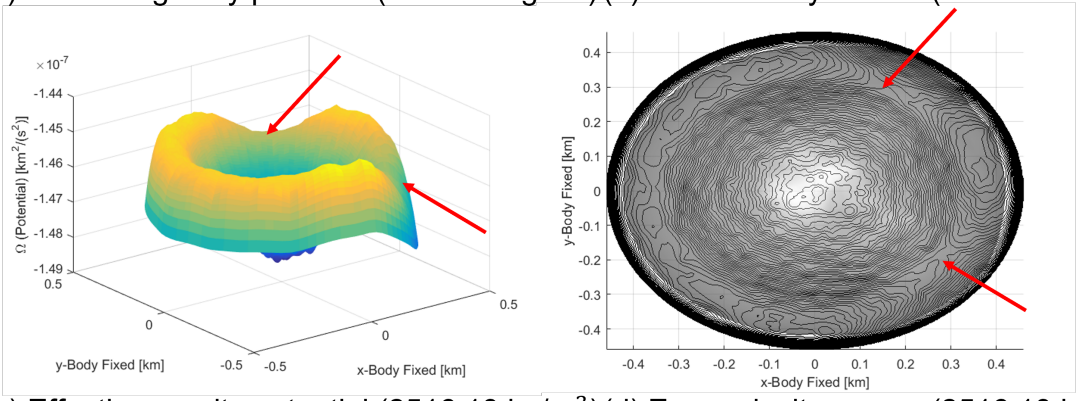

(c) Effective gravity potential (2516.18 kg/m^3) (d) Zero velocity curves (2516.18 kg/m^3)

Figure 7: Effective gravity potential and zero velocity curves for a rubble-pile with denser core as shown in Fig. 5.c-.d. .

Table 6: Didymos's normalised $\bar{C}_{nm}$ gravity coefficients associated to the internal structure of Fig. 5 .

n	m	$\bar{C}_{nm}$ (Fig. 5.a)	$\bar{C}_{nm}$ (Fig. 5.b)	$\bar{C}_{nm}$ (Fig. 5.c)	$\bar{C}_{nm}$ (Fig. 5.d)
1	0	+3.063060644183e-04	+4.117639321938e-04	+2.739152056391e-04	+1.864367610684e-04
1	1	+1.722436179532e-03	+1.849480310899e-03	+1.604318047499e-03	+1.502579666750e-03
2	0	-4.502150215652e-02	-4.838611557664e-02	-4.246952607820e-02	-3.974854271949e-02
2	1	+6.740475358382e-04	+7.236240039477e-04	+6.345040087647e-04	+5.945006905785e-04
2	2	+5.156593052720e-04	+5.560366902186e-04	+4.856435296781e-04	+4.529619980740e-04
3	0	+1.850936209402e-06	-2.269094742726e-06	+2.573806035246e-06	+6.016427290019e-06
3	1	-1.085521396822e-03	-1.164465794630e-03	-1.025809785439e-03	-9.619593292093e-04
3	2	-2.133564039241e-04	-2.370135702644e-04	-2.029307978555e-04	-1.834525604139e-04
3	3	-1.879815801043e-03	-2.019062429368e-03	-1.772476235004e-03	-1.659946129615e-03
4	0	+6.768234043185e-03	+7.277178526624e-03	+6.383617063853e-03	+5.971965803738e-03
4	1	-2.901532329806e-04	-3.073142846011e-04	-2.740264825580e-04	-2.602916196263e-04
4	2	+2.485268031458e-04	+2.645780592116e-04	+2.334955690833e-04	+2.206465069434e-04
4	3	-4.214277942546e-04	-4.503994016101e-04	-3.969453125282e-04	-3.736314181083e-04
4	4	-1.501534189310e-03	-1.615569387408e-03	-1.416151741159e-03	-1.323879595199e-03
5	0	+8.014768591060e-05	+8.477603743627e-05	+7.562849235785e-05	+7.193201400912e-05
5	1	+6.370027705096e-05	+6.817714415869e-05	+5.987355711028e-05	+5.627296087217e-05
5	2	-2.138460002224e-04	-2.310501314638e-04	-2.017427989004e-04	-1.877861194279e-04
5	3	+6.401841048075e-04	+6.868054247584e-04	+6.041410592159e-04	+5.664695483829e-04
5	4	-8.152829068264e-04	-8.758589708810e-04	-7.690136723503e-04	-7.200403660151e-04
5	5	-3.622702059541e-04	-3.902998032443e-04	-3.417470102826e-04	-3.190453514083e-04

Table 7: Didymos's normalised $\bar{S}_{nm}$ gravity coefficients associated to the internal structure of Fig. 5 .

n	m	$\bar{C}_{nm}$ (Fig. 5.a)	$\bar{C}_{nm}$ (Fig. 5.b)	$\bar{C}_{nm}$ (Fig. 5.c)	$\bar{C}_{nm}$ (Fig. 5.d)
1	0	+0.000000000000e+00	+0.000000000000e+00	+0.000000000000e+00	+0.000000000000e+00
1	1	+9.857551849453e-04	+1.098849837079e-03	+9.261512170353e-04	+8.334842825820e-04
2	0	+0.000000000000e+00	+0.000000000000e+00	+0.000000000000e+00	+0.000000000000e+00
2	1	+2.210138460704e-03	+2.381172881058e-03	+2.079915674552e-03	+1.941622026208e-03
2	2	-3.000359245388e-04	-3.231078566844e-04	-2.857308001565e-04	-2.669251390297e-04
3	0	+0.000000000000e+00	+0.000000000000e+00	+0.000000000000e+00	+0.000000000000e+00
3	1	+3.850169054184e-04	+4.035376564593e-04	+3.629056342238e-04	+3.482995003845e-04
3	2	+2.104377813839e-03	+2.255800058256e-03	+1.983383764715e-03	+1.861210891667e-03
3	3	-1.595882009930e-03	-1.713127588804e-03	-1.503199600131e-03	-1.408555457727e-03
4	0	+0.000000000000e+00	+0.000000000000e+00	+0.000000000000e+00	+0.000000000000e+00
4	1	-6.748719244595e-04	-7.247017563787e-04	-6.366782316758e-04	-5.963989356010e-04
4	2	+1.859984921921e-05	+2.274774045826e-05	+1.795167874934e-05	+1.448210924976e-05
4	3	+4.088279674128e-04	+4.377427002255e-04	+3.849591676460e-04	+3.616649679237e-04
4	4	-1.454881483757e-03	-1.563848535051e-03	-1.372273639643e-03	-1.284149433241e-03
5	0	+0.000000000000e+00	+0.000000000000e+00	+0.000000000000e+00	+0.000000000000e+00
5	1	+8.014138381291e-05	+8.665363522305e-05	+7.601769358177e-05	+7.071359568326e-05
5	2	-1.074829259259e-04	-1.147227708959e-04	-1.013824710832e-04	-9.555564690086e-05
5	3	+9.846797468152e-05	+1.066708277101e-04	+9.282262165891e-05	+8.616235867271e-05
5	4	-9.030681646278e-04	-9.730332440791e-04	-8.518452509905e-04	-7.951790693106e-04
5	5	-5.287633286939e-04	-5.668767529352e-04	-4.987830513801e-04	-4.680099172457e-04

Conclusion: In this article, the dynamical stability of PKDGRAV rubble-pile models has been studied. The mascons gravity model has served as benchmark to compare several models and gain information of gravity coefficients and dynamical stability (i.e., equilibrium points). The aim is to then extend the study to other rubble-pile models as SPH and multi-polyhedron models. It has been demonstrated the importance in the mascons resolution for the accuracy in the gravity coefficients and location of equilibrium points. The polyhedron gravity model was used as true model when selecting the mascons resolution for a homogeneous bulk density asteroid. It was evaluated that 1.2M mascons provide with a good accuracy withing the navigation tolerance. In order to overcome the ambiguity in the gravity coefficients, it has been demonstrated that it is possible to further constraints the internal structure solution by looking at the effective potential and the dynamical stability. The rubble-pile models here analysed present non uniformly distributed voids when compared with the polyhedron case or homogeneous mascons case which affects the dynamical stability and gravity coefficients. For denser core rubble-piles, it was still possible to identify a ridge in the effective potential right below a thin substrate material under the surface where regions of stability and instability could be identified. The evaluation of the dynamical properties of Didymos constrains the assumption made for the internal structure and provides a direct comparison of models. Moreover, this study provides a database of expected gravity estimates that is beneficial for the inverse problem of estimation of the asteroid internal properties from Hera's gravity measurements during the Juventas CubeSat radio science campaign.

Acknowledgement: SS was funded by UKRI-FLF grant number MR/W009498/1.

References: [1] R. T. Daly, et al. (2023) *Nature* 1–3. [2] E. Dotto, et al. (2021) *Planetary and Space Science* 199:105185. [3] S. Watanabe, et al. (2019) *Science* 364:268. [4] S. Soldini, et al. (2020) *Planetary and Space Science* 180:104740 ISSN 0032-0633 doi. [5] P. Michel, et al. (2018) *Advances in Space Research* 62(8):2261. [6] H. R. Goldberg, et al. (2019) . [7] D. S. Lauretta, et al. (2019) *Science* 366(6470) ISSN 0036-8075 doi. arXiv:https://science.sciencemag.org/content/366/6470/eaay3544.full.pdf. [8] M. Hirabayashi, et al. (2022) *The Planetary Science Journal* 3(6):140 doi. [9] Y. Zhang, et al. (2017) *Icarus* 294:98 ISSN 0019-1035 doi. [10] Y. Zhang, et al. (2021) *Icarus* 362:114433 ISSN 0019-1035 doi.